J Mater Sci (2009) 44:6727–6735
DOI 10.1007/s10853-009-3566-9

MESOSTRUCTURED MATERIALS

Surface properties and epoxidation catalytic activity of Ti-SBA15 prepared by direct synthesis

François Bérubé · Freddy Kleitz · Serge Kaliaguine

Received: 1 December 2008 / Accepted: 12 May 2009 / Published online: 9 June 2009

Abstract The influence of hydrothermal treatment time on the physicochemical properties and the catalytic activity in cyclohexene epoxidation of titanium-substituted SBA15 silicas prepared by direct one-step synthesis was systematically studied using a combination of N_2 physisorption at −196 °C, X-ray diffraction, X-ray photoelectron spectroscopy, diffuse reflectance UV–Vis, and elemental analysis. The other synthesis parameters were chosen to illustrate the different chemical environments of the titanium species formed before, during, and after the precipitation of anatase TiO_2. At the beginning of hydrothermal treatment, results showed that the titanium species are homogeneously dispersed in the silica framework. When anatase TiO_2 clusters precipitate, they do so mainly on the external surface of the mesoporous material. At higher hydrothermal treatment times, the material showed a decreased catalytic activity even if essentially no variation in their specific surface area was then observed. This lower activity was shown to be due to a partial coverage of active tetrahedral Ti species by extraframework higher coordination TiO_2 deposit.

Introduction

The discovery of titanium silicates [1–4] with both MFI (TS-1) and MEL (TS-2) structures opened the perspective of zeolitic materials as oxidation catalysts. Several reactions of partial oxidation of organic reactants using dilute solution of hydrogen peroxide could, for the first time, be performed selectively in very mild conditions [5, 6]. Nevertheless, despite their excellent performances, these zeolitic oxidation catalysts have some limitations. The bulky molecules of tri-alkylmonoaromatics or even polyaromatics, whose kinetic diameters are higher than 0.55 nm, are indeed not accessible to the internal pore system of these zeolite-type materials.

To overcome the traditional limitations of zeolites, several studies have been initiated in the field of mesoporous molecular sieves, beginning with the M41S family [7]. The pore diameters of these new solids have been tuned in the mesoporous range ($2 < d < 50$ nm), which make them suitable for processes involving diffusion of bulky molecules to internal active sites. Since the early syntheses of MCM-41, new mesostructured materials exhibiting a large variety of structures and pore sizes [8–11] have been developed. One of the most promising developments in this research field was the discovery of SBA15 materials by Zhao et al. in 1998 and synthesized using nonionic triblock-copolymer as structure-directing agent in acidic medium [12, 13]. Compared with the previous M41S family, the SBA15-type silica shows an enhanced hydrothermal stability because of thicker silica walls [14, 15] and also shows larger pore size (6–12 nm). However, the main problem associated with the mesoporous molecular sieves is their amorphous silica walls, which greatly limits their use as catalytic supports [16, 17].

Recently, many efforts have been made to incorporate heteroelements into mesoporous molecular sieves to give them new catalytic properties [15–24]. In the case of titanium, several post-synthesis grafting methods such as the gaseous $TiCl_4$ grafting [25, 26] and the nonaqueous post-

F. Bérubé · S. Kaliaguine (✉)
Chemical Engineering Department, Laval University, Quebec City, QC G1V 0A6, Canada
e-mail: serge.kaliaguine@gch.ulaval.ca

F. Kleitz
Chemistry Department, Laval University, Quebec City, QC G1V 0A6, Canada
e-mail: freddy.kleitz@chm.ulaval.ca

impregnation with Ti alkoxides [27–29], $Ti[OSi(OC_2H_3)_4]_4$ molecular precursors [30], and others titanocenes complexes [31–33] have been carried out. However, these post-synthesis methods sometimes lead to the formation of metal oxides in the channels or on the external surface of the catalysts. To avoid these problems, several attempts have been made to incorporate titanium into the silica framework of MCM41 [34–36], MCM48 [37–40], HMS [41, 42], MSU [43–45], SBA1 [46–48], and SBA15 [49–55] mesostructured materials by direct one-pot synthesis. In the case of Ti-SBA15, only a small fraction of the titanium precursor added was retained into the mesoporous structure, which might be due to the easy dissociation of metal–O–Si bonds under these strongly acidic conditions. Several optimization methods have been considered to increase loading of isolated Ti^{4+} into the silica framework, such as fluoride addition [49], microwave hydrothermal treatment [50], and pH adjustment of the synthesis solution [51]. However, in cases where high titanium substitution was obtained, a formation of extraframework TiO_2 was also observed [52].

Several works showed that the synthetic parameters greatly influence the substitution of titanium in SBA15 materials [52–54]. In our previous study, the influences of hydrochloric acid concentration, silicon precursor concentration, and hydrothermal treatment temperature and time on the Ti incorporation ratio and its chemical environment were systematically studied over a wide range of titanium content in the initial gel mixture [52]. It was shown that when the isolated titanium species present in the gel reach a critical concentration, an increase in incorporation ratio is observed due to the formation of anatase TiO_2 clusters on the materials surface. It was also found that this critical titanium loading is mainly influenced by synthesis temperature, hydrothermal treatment time, and silicon precursor concentration, and does not depend on acid concentration. Although the conditions that lead to the anatase TiO_2 formation are well known, few details about the different steps of this crystallization process were obtained.

In this study, the influence of the anatase TiO_2 formation on the physicochemical properties and the catalytic activity in cyclohexene epoxidation of titanium-substituted SBA15 prepared by direct synthesis (co-condensation) is reported. The initial molar gel compositions have been chosen to obtain a marked precipitation of anatase TiO_2 after the hydrothermal treatment of the material.

Experimental section

Materials

Ti-SBA15 materials were synthesized using Pluronic P123 (Aldrich, $M_w = 5800$ g/mol) as a structure-directing agent, tetraethylorthosilicate (TEOS 98%, Aldrich) as a silicon source, and tetrapropylorthotitanate (TPOT 97%, Aldrich) as titanium precursor. The synthesis was carried out with the following initial molar gel composition: 0.99 TEOS/0.10 TPOT/0.54 HCl/0.016 P123/100 H_2O. In a typical synthesis, 6.0 g of Pluronic P123 was dissolved in 114 g of deionized water and 3.5 g of hydrochloric acid (37%) at 35 °C under magnetic stirring. Then, 13.0 g of TEOS and 1.8 g of TPOT were premixed and rapidly added to the initial homogeneous solution to obtain a Ti/Si atomic ratio of 10% in the initial gel. The resulting mixture was stirred for 24 h at 35 °C and subsequently hydrothermally treated for a given time at 60 °C to ensure further framework condensation. The solid products were recovered by filtration and dried in air at 100 °C for 24 h. Finally, the products were calcined at 550 °C for 3 h to remove the template. Calcined titanosilicate samples are designated as Ti-SBA15(t) were t stands for the hydrothermal treatment time at 60 °C.

Characterization

Wide angle XRD patterns were recorded on a Philips PW1011 diffractometer and CuKα radiation ($\lambda = 1.5496$ Å). The reference pattern of crystalline anatase was obtained from the Powder Diffraction File 2 (PDF-2) database licensed by the International Center for Diffraction Data (ICDD).

Elemental analysis was performed by atomic absorption using a M1100B Perkin-Elmer atomic absorption spectrophotometer. Nitrogen adsorption and desorption isotherms were determined at −196 °C using an ASAP 2010 sorption analyzer. Prior to analysis, samples were outgassed at 250 °C for 12 h under vacuum. Specific surface area, S_{BET}, was determined using BET equation over the relative pressure range of 0.05–0.2. The pore size distributions were obtained by the nonlocal density functional theory (NLDFT) method and calculated using the Autosorb-1 1.52 software supplied by Quantachrome Instruments. The kernel selected was N_2 on silica at −196 °C assuming cylindrical pore geometry and the metastability model based on the adsorption branch [56]. Micropore volume was determined from NLDFT cumulative pore volumes estimated for pores smaller than 2 nm. Diffuse reflectance UV–Vis (DRUV) spectra were recorded using a Varian Cary 500 spectrophotometer equipped with a praying mantis. A spectralon® reflectance standard was used as reference.

X-ray photoelectron spectra were collected on a Kratos Axis-Ultra electron spectrometer (UK) using a monochromatic Al Kα X-ray source at a power of 300 W and operated with a base pressure of 5×10^{-10} Torr. Charge compensation was required using a low-energy electron

beam perpendicular to the surface of the samples. Survey spectra used for determining the elemental composition were collected at pass energy of 160 eV. High-resolution spectra of Ti(2p) and O(1s) were collected in conditions giving a nominal energy resolution of 0.5 eV as measured on $Ag3d_{5/2}$ (pass energy of 20 eV). High-resolution spectra of C1s were collected with pass energy of 40 eV giving a nominal resolution of 0.6 eV. Linear background substraction was used for the curve fitting of Ti(2p) spectra, and the O(1s) and Ti(2p) binding energies were referenced to the C(1s) line situated at 285.0 eV. All fittings were performed using the Casa XPS software.

The epoxidation of cyclohexene was chosen as the test reaction, and the experimental conditions used were similar to a previously published procedure [57]. Twenty mmol of cyclohexene, 4 mmol of TBHP (90% in H_2O), 10 mL of acetonitrile, and 0.1 g of catalyst were mixed in a 50-mL round-bottom flask and were heated to 70 °C under stirring for 3 h. The products were analyzed by gas chromatography (Fisons GC8000 equipped with a Varian CP-SIL capillary column and coupled with a Fisons MD800 mass spectrometer).

Results

Some physicochemical properties of the Ti-SBA15 materials are reported in Table 1. The 5.4% Ti/Si atomic ratio of the solid product recovered after the initial synthesis step at 35 °C (24 h) corresponds to 54% of the titanium precursor introduced in the initial synthesis mixture. Thus, the Ti precipitates simultaneously with Si species during synthesis. Then, up to 9 h of aging, the Ti/Si ratio varies very little up to 6%. This indicates that the rate of Ti precipitation is quite low in this initial period. For longer hydrothermal treatment times, a steep increase in the titanium loading of the materials was observed. Ti-SBA15(24) sample showed a Ti/Si atomic ratio of 9.2% which corresponds to 92% of the titanium precursor present in the initial synthesis gel. Then, the Ti/Si atomic ratio of the solid product only increased slightly up to 96 h indicating that some titanium species remain stable in solution under these conditions.

N_2 adsorption-desorption isotherms at −196 °C before and after 96 h of hydrothermal treatment at 60 °C are shown in Fig. 1. All the Ti-SBA15 materials synthesized in this study show a type-IV isotherm with a low capillary condensation step and a triangular hysteresis loop of type H2. Furthermore, the shape of the hysteresis loop with a slanted adsorption branch and a steep vertical capillary evaporation at $P/P_0 = 0.45$ indicates that the cylindrical pores of SBA15 have pronounced surface rugosity associated with a corona of noninterconnecting micropores [58–61]. All these characteristics are those of SBA15 materials synthesized at relatively low aging temperatures (<60 °C). Interestingly, the adsorption capacity of N_2 at high relative pressures ($P/P_0 > 0.7$) is more important for Ti-SBA15(96). This result may indicate some slight agglomeration of SBA15 particles associated to the presence of TiO_2 clusters at the external surface of the particles and/or at pore mouth. The evolution of the specific surface area presented in Table 1 indicates that the hydrothermal treatment induces an increase in specific surface area. This phenomenon was reported before and could be attributed to the increase in the micro- and mesopore volume [58] and the rearrangement of the silica walls provoked by enhanced silanol condensation during the hydrothermal aging treatment.

Wide-angle X-ray diffraction (XRD) patterns of Ti-SBA15 are presented in Fig. 2. No crystalline phase was detected by XRD for material aged at 60 °C up to 9 h. For samples aged for a longer time ($t \geq 12$ h), wide-angle

Table 1 Textural properties of Ti-SBA15 synthesized with different hydrothermal treatment times at 60 °C

Sample	Aging time (h)	Ti/Si[a] (%)	S_{BET} (m^2/g)	V_{mic}[b] (cm^3/g)	Pore volume[c] (cm^3/g)	D_p[d] (nm)
Ti-SBA15(0)	0	5.4	595	0.079	0.52	5.7
Ti-SBA15(3)	3	5.5	632	0.076	0.52	5.6
Ti-SBA15(6)	6	5.7	645	0.088	0.53	5.8
Ti-SBA15(9)	9	6.0	666	0.089	0.53	5.6
Ti-SBA15(12)	12	8.1	649	0.086	0.53	5.8
Ti-SBA15(24)	24	9.2	706	0.099	0.53	5.8
Ti-SBA15(48)	48	9.4	728	0.093	0.60	5.9
Ti-SBA15(96)	96	9.4	717	0.084	0.61	6.0

[a] Atomic ratio Ti/Si determined by elemental analysis

[b] Micropore volume determined from NLDFT calculations

[c] Volume of nitrogen adsorbed at $P/P_0 = 0.95$

[d] Pore diameter determined by NLDFT calculations taking into account the adsorption branch

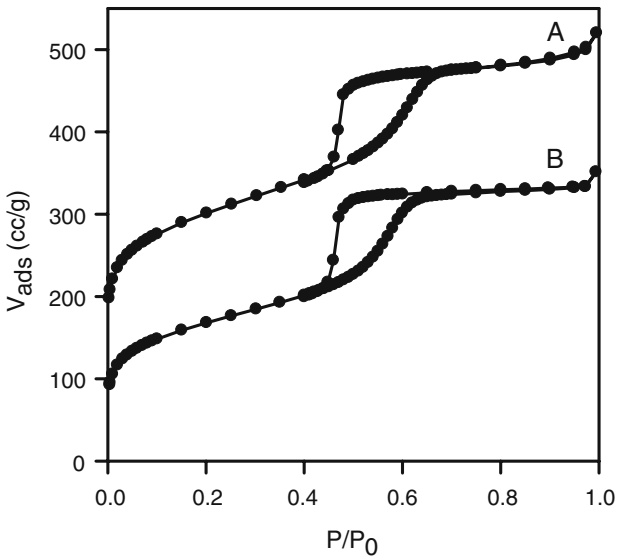

Fig. 1 N_2 sorption isotherms at −196 °C obtained on Ti-SBA15 treated hydrothermally at 60 °C for 0 (*A*) and 96 h (*B*). Isotherm *A* is shifted by 100 cm^3/g

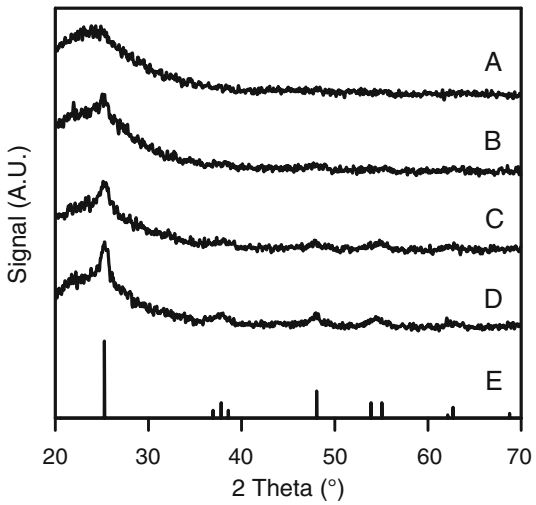

Fig. 2 Wide angle XRD patterns of calcined Ti-SBA15 treated hydrothermally at 60 °C for 9 (*A*), 12 (*B*), 24 (*C*), and 96 h (*D*). The reference pattern of anatase TiO_2 is given as *E*

XRD spectra showed weak reflections characteristic of the anatase TiO_2 structure. Just like in our previous study, the measured steep increase in the titanium deposition ratio is associated with the formation of anatase TiO_2 [52]. Moreover, the relative intensity of the signal associated with this crystalline phase compared to those associated with amorphous silica ($2\theta = 20°$–$30°$) increased with the hydrothermal treatment time.

DRUV spectra of Ti-SBA15 samples treated at 60 °C for different aging times are presented in Fig. 3. A band between 200 and 240 nm is attributed to a ligand-to-metal

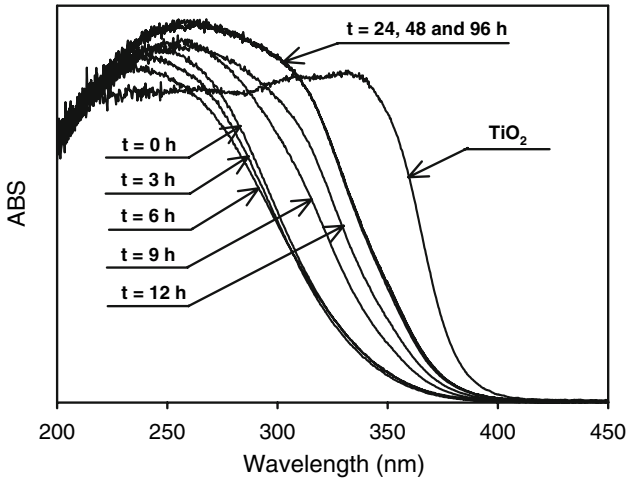

Fig. 3 UV–Vis diffuse reflectance spectra of calcined Ti-SBA15 synthesized with different hydrothermal treatment times at 60 °C

charge-transfer transition in isolated TiO_4 units [62]. In the case of titanosilicate materials, this feature is associated to Ti^{4+} species in tetrahedral coordination incorporated into the silica framework. The DRUV spectrum of anatase TiO_2 (Fig. 3) indicates that a band centered at 330 nm is attributed to a ligand-to-metal charge-transfer of titanium in octahedral coordination [62–64]. Reflectance bands between these two wavelength values may be assigned to titanium in intermediate coordination and to small TiO_2 clusters through quantum size effect [62, 65, 66].

For Ti-SBA15 samples aged for less than 9 h, DRUV spectra showed a large band centered at 230–250 nm and extending up to 370 nm, suggesting that small TiO_2 clusters and/or penta-coordinated titanium species are present in the materials. Moreover, there is no substantial change in the spectra of these three samples, indicating that the chemical environment of the TiO_2 species in the silica framework does not vary before the precipitation of anatase TiO_2. Then, the DRUV spectra of samples aged between 9 and 24 h showed that the absorption signal at wavelength higher than 330 nm increased drastically due to the formation of bulk anatase TiO_2. Further increase in the duration of hydrothermal treatment had no influence on UV absorption.

A comparison between the Ti/Si atomic ratios of Ti-SBA15 samples measured by both atomic absorption and X-ray photoelectron spectroscopy (XPS) is presented in Fig. 4. The Ti/Si ratio measured by XPS plotted as a function of the bulk Ti/Si measured by atomic absorption is also shown in Fig. 5. For the samples synthesized at low hydrothermal treatment times ($t \leq 3$ h), titanium-over-silicon molar ratios measured by both methods were similar suggesting titanium species homogeneously dispersed in the silica framework. During anatase TiO_2 precipitation, one can see that the measured increase in the concentration

of titanium species $(Ti/Si)_{XPS}$ detected by XPS and therefore located in the vicinity of the external surface of the particles, follows substantially the same evolution with aging time as the bulk value (Fig. 4). However, one can see that the Ti/Si ratio measured by XPS is much higher than the bulk Ti/Si ratio for samples aged for more than 3 h. This result indicates some Ti surface segregation suggesting that the precipitated anatase TiO_2 is located predominantly on the external surface of the particles.

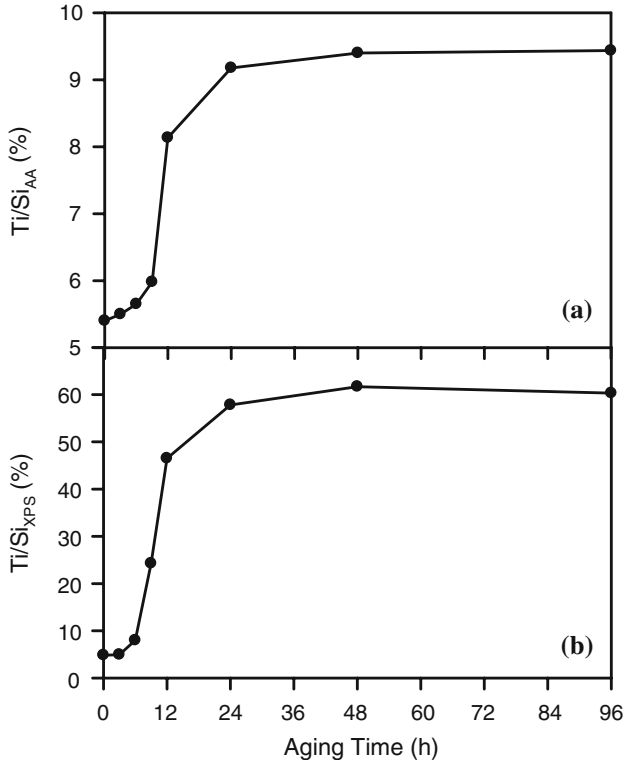

Fig. 4 Ti/Si atomic ratios measured by atomic absorption spectroscopy (**a**) and by XPS (**b**) obtained on Ti-SBA15 synthesized with different hydrothermal treatment times at 60 °C

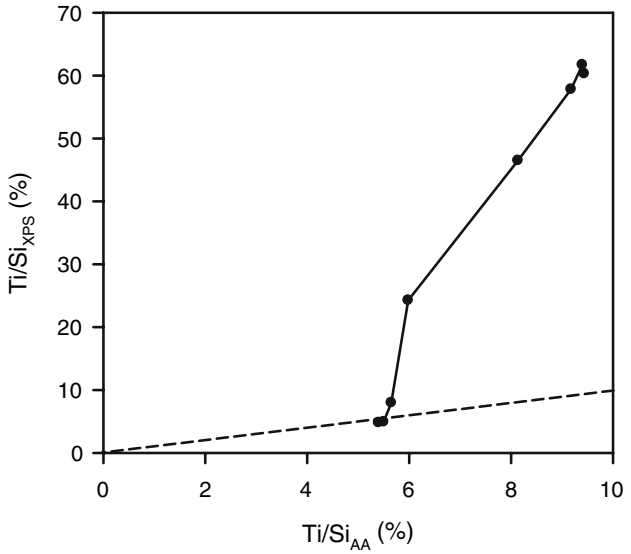

Fig. 5 Ti/Si atomic ratio measured by XPS as a function of Ti/Si atomic ratios measured by atomic absorption spectroscopy obtained on Ti-SBA15 synthesized with different hydrothermal treatment times at 60 °C

Figure 6 shows O(1s) XPS spectra of Ti-SBA15 synthesized at 60 °C for different hydrothermal treatment times. The binding energy associated with the different oxygen species lines and the relative intensity of their signal are reported in Table 2. For Ti-SBA15 samples synthesized with an hydrothermal treatment time lower than 9 h, only one line centered at 533.1 eV (HBE) appears on the O(1s) XPS spectra. This feature was observed for siliceous SBA15 and titanosilicate materials with titanium dispersed in the silica framework [29]. For samples aged for longer times ($t \geq 9$ h), another line at 530.2 eV (LBE)

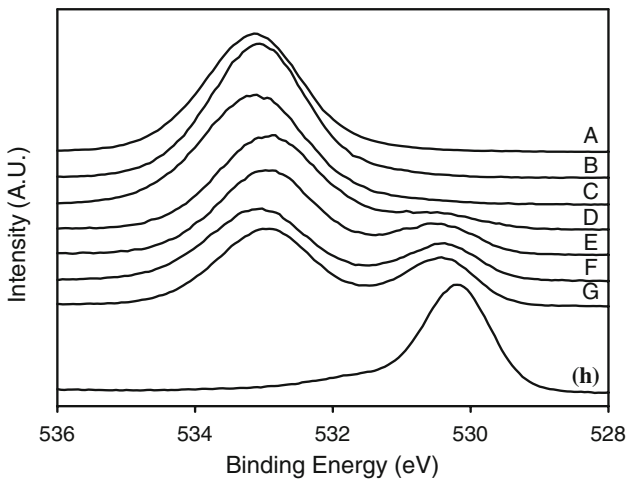

Fig. 6 O(1s) XPS spectra of Ti-SBA15 treated hydrothermally at 60 °C for 0 (*A*), 3 (*B*), 6 (*C*), 9 (*D*), 12 (*E*), 48 (*F*), and 96 h (*G*). The reference spectrum of anatase TiO_2 is given as *H*

Table 2 O(1s) binding energies and relative intensities of Ti-SBA15 synthesized with different hydrothermal treatment times at 60 °C

Sample	Binding energies (eV)		Relative intensities (%)	
	LBE	HBE	LBE	HBE
Ti-SBA15(0)	533.2	–	100	0
Ti-SBA15(3)	533.1	–	100	0
Ti-SBA15(6)	533.2	–	100	0
Ti-SBA15(9)	533.0	530.6	85.4	14.6
Ti-SBA15(12)	533.0	530.5	78.0	22.0
Ti-SBA15(24)	533.0	530.6	67.3	32.7
Ti-SBA15(48)	533.0	530.5	68.3	31.7
Ti-SBA15(96)	533.1	530.4	72.4	27.6
Anatase TiO_2	–	530.2	0	100

LBE and HBE are, respectively, defined as the lines at low binding energy and high binding energy observed on the O(1s) XPS spectra

appeared, which is associated to bulk anatase TiO_2 (see Fig. 6, curve H). The increased Ti/Si molar ratio with aging time results in a continuous increase in intensity of the 530.2 eV line. A maximum value of the fraction of the O(1s) signal in this band is observed after 24 h of aging time (32.7%) and followed by a minor decrease (to 27.6%) which is likely associated with the increased anatase crystallinity (see Fig. 2) and surface sintering of TiO_2 clusters.

Ti(2p) XPS spectra of Ti-SBA15 treated at 60 °C for different aging durations are presented in Fig. 7. For the sake of clarity, only the Ti($2p_{3/2}$) peaks are shown, and the position and the full width at half maximum (FWHM) of these peaks are presented in Fig. 8. Several systematic Ti(2p) XPS investigations of TiO_2–SiO_2 mixed oxide over a wide range of TiO_2 content showed that these lines are very sensitive to the coordination of titanium species [29, 67, 68]. At low TiO_2 loading, our solid samples show essentially tetrahedral titanium with a $Ti_{2p3/2}$ binding energy close to 460 eV, whereas this binding energy decreased down to 459.0 eV with the appearance of anatase TiO_2. The latter line is associated with octahedral titanium species.

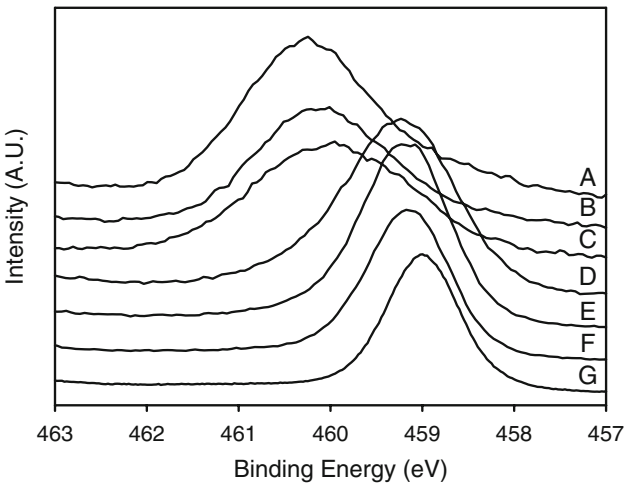

Fig. 7 Ti(2p) XPS spectra of Ti-SBA15 treated hydrothermally at 60 °C for 0 (*A*), 3 (*B*), 6 (*C*), 9 (*D*), 12 (*E*), and 96 h (*F*). The reference spectrum of anatase TiO_2 is given as *G*

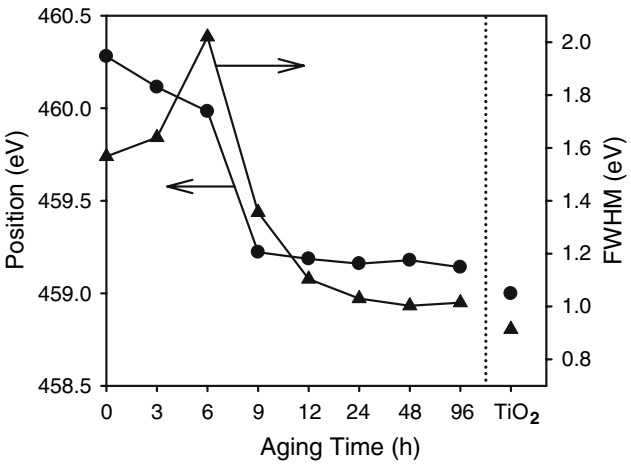

Fig. 8 Maximum binding energy position (*triangles*) and FWHM (*circles*) of Ti($2p_{3/2}$) peaks measured by XPS and obtained for Ti-SBA15 synthesized with different hydrothermal treatment time at 60 °C

For the sample synthesized without hydrothermal treatment ($t = 0$ h), Ti(2p) XPS spectrum shows a broad Ti($2p_{3/2}$) peak centered at 460.3 eV. Other studies of Ti-SBA15 with low titanium loading also showed similar results for titanium species in tetrahedral coordination, indicating that no bulk anatase TiO_2 is detected on the material surface [29, 67]. For samples recovered within the first 6 h of hydrothermal treatment (0 h $< t \leq$ 6 h), the binding energies corresponding to Ti($2p_{3/2}$) line slightly decreased and the FWHMs of these peaks increased (see Fig. 8). The Ti(2p) XPS spectra corresponding to these samples (Fig. 7, curves B and C) also exhibit an asymmetry toward lower binding energy, suggesting a slight increase in the coordination number of titanium species located on the external surface of the material. However, the Ti(2p) XPS spectrum of Ti-SBA15(6) reveals a binding energy of 460.0 eV for Ti($2p_{3/2}$) line, which is only 0.3 eV lower than the one of the sample synthesized without hydrothermal treatment. It is therefore believed that most of the titanium species present on the external surface of Ti-SBA15(6) sample are constituted of isolated tetrahedral TiO_2 clusters incorporated in the silica framework. Then, between 6 and 9 h of aging at 60 °C, Ti(2p) XPS results clearly showed that the chemical environment of the titanium species detected changed drastically. The Ti(2p) spectrum of Ti-SBA15(9) indeed shows more characteristics of the anatase TiO_2 spectrum (Fig. 7, curve G) exhibiting a binding energy of 459.2 eV for the Ti($2p_{3/2}$) line. Moreover, for this sample, the signal corresponding to the titanium species in tetrahedral coordination has almost vanished. However, the high FWHM of this peak and the shoulder toward the higher binding energy suggests that some titanium moieties can be still associated with titanium in intermediate coordination. Then, for samples aged for longer hydrothermal treatment times ($t > 9$ h), the position of Ti($2p_{3/2}$) peaks remains essentially the same and the latter become narrower.

It is well known that the epoxidation of cyclohexene with hydroperoxides only possible over TiO_2–SiO_2 mixed oxides that contain titanium in tetrahedral coordination [6, 69, 70]. Thus, the conversion of cyclohexene is in direct relation with the concentration of these active titanium sites in the materials. To establish a relation between the nature of titanium species and the catalytic activity, a comparison between the specific surface area and the conversion of

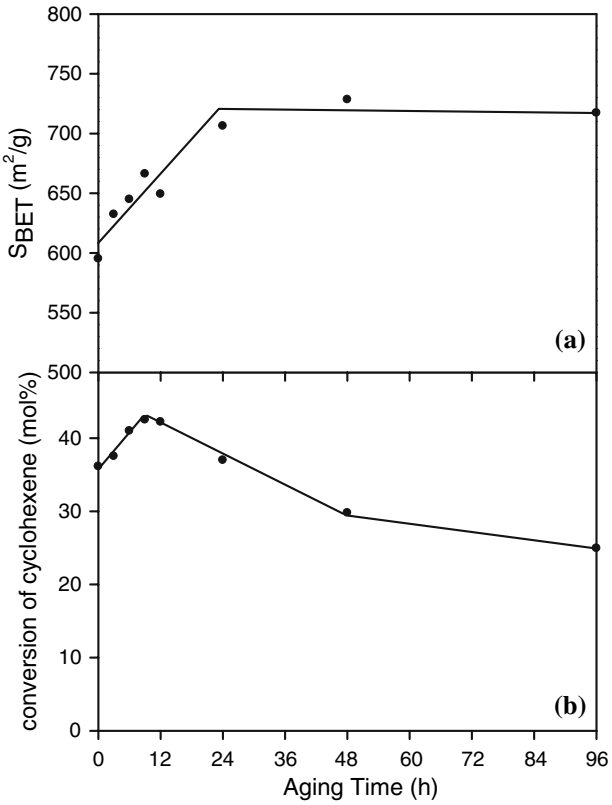

Fig. 9 Specific surface area (**a**) and conversion of cyclohexene (**b**) for Ti-SBA15 synthesized with different hydrothermal treatment times at 60 °C

cyclohexene reached after 3 h of reaction at 70 °C for the different Ti-SBA15 materials is presented in Fig. 9. For this reaction, the major product was cyclohexene oxide and the secondary products were mostly 2-cyclohexene-1-ol and possibly 2-cyclohexene-1-one. In all cases, the selectivity for cyclohexene oxide was around 95%. It was shown that the conversion of cyclohexene increases proportionally to the specific surface area for samples aged between 0 and 12 h. A maximal conversion of 43% was obtained for Ti-SBA15(9). This value is similar to those obtained by Hua et al. on Ti-SBA15 materials considering the lower amount of catalyst (0.1 g instead of 0.2 g) used in our study [57]. For samples synthesized with higher hydrothermal treatment times, decreasing cyclohexene conversions were observed despite the slight increase in specific surface area. This result indicates a decrease in the density of titanium species that are active for the epoxidation of cyclohexene.

Discussion

All the above results show that the physicochemical properties and the catalytic activity in epoxidation of cyclohexene of Ti-SBA15 prepared by direct synthesis are greatly influenced by the possible precipitation of the anatase TiO_2 during hydrothermal treatment. For low aging treatment times ($t \leq 6$ h), XRD and O(1s) and Ti(2p) XPS spectra reveal that there is no anatase TiO_2 in the recovered solid products. DRUV experiments also showed that titanium species present in the materials are mostly constituted of isolated tetrahedral titanium species possibly accompanied by traces of small clusters of Ti in higher coordination to oxygen. Moreover, the Ti/Si atomic ratios measured by XPS, which are substantially the same as those measured by atomic absorption for these samples, also suggest that titanium is uniformly dispersed into the silica framework and showing no surface segregation.

Further increase in the aging time leads to a drastic increase in the titanium content which suggests a TiO_2 precipitation over the solid. XRD, DRUV, and XPS measurements indicated that the measured increase in the titanium loading can be attributed to the deposition of higher coordination titanium oxide species with appearance of anatase TiO_2 crystalline phase after 12 h. Moreover, the sudden increase in the Ti/Si ratio measured by XPS compared to the bulk Ti/Si ratio indicates that the TiO_2 precipitation occurred mainly on the external surface of the particles. At aging times higher than 24 h, the increased N_2 adsorption at higher relative pressures is associated with the external surface deposition of this TiO_2 phase suggesting some particle agglomeration creating interparticular macropores. Interestingly, the line on the Ti(2p) XPS spectra associated with the titanium in tetrahedral coordination (around 460 eV BE) essentially disappeared between 6 and 9 h. This feature could not be attributed to a complete coverage of the SBA15 particles' external surface since the HBE O(1s) line associated with the oxygens bounded to silicon atoms still represent 85% of the relative signal for Ti-SBA15(9) sample. It appears thus that the high coordination TiO_2 phase deposited after 9 h aging time is precisely localized on the tetrahedral surface lattice of Ti species. This suggests that the isolated tetrahedral Ti species act as surface nuclei for the deposition of the new TiO_2 phase. This would provide an explanation for the decreased epoxidation activity with aging time since the tetrahedral Ti species involved as nuclei are no longer accessible to the reactants.

For hydrothermal treatment durations higher than 12 h, Ti(2p) XPS results showed no substantial change in the chemical environment of TiO_2 species located on the external surface. However, even if the specific surface area of the materials reached a maximal value during this period, the specific activity for the epoxidation of cyclohexene decreased. This decrease in the specific activity after 12 h is obviously related to the decreasing fraction of tetrahedral Ti species as discussed above.

Conclusion

In summary, the physicochemical properties and the catalytic activity in epoxidation of cyclohexene were studied as a function of the time of hydrothermal treatment of titanium-substituted SBA15 materials prepared by direct synthesis. In the selected aging conditions, a progressive precipitation of TiO_2 clusters follows the initial incorporation of Ti species during Ti-SBA15 synthesis step. The results suggested that the isolated titanium species present on the surface of the material could initiate the crystallization of anatase TiO_2 clusters. On long-term hydrothermal treatment durations, it was also shown that this disappearance of the tetrahedrally coordinated titanium leads to a decrease in the specific activity for the epoxidation of cyclohexene. In the case of mesoporous TiO_2–SiO_2 mixed oxide, it is thus clear that the hydrothermal aging time should be optimized to obtain more active epoxidation catalysts.

Acknowledgements The authors wish to thank NSERC for financial support. The authors are grateful to Mr. G. Lemay for assistance in the experimental part. We thank Professor M. Leclerc from the Chemistry Department of Laval University for access to UV–Vis spectrometer. We also thank Dr A. Adnot for XPS measurements and valuable discussions.

References

1. Taramasso M, Perego G, Notari B (1983) US Patent 4 410 501
2. Lam Shamleen KK (1985) US Patent 4 623 526; (1985) US Patent 4 519 998; (1984) European Patent B1 0 148 038
3. Reddy JS, Kumar R, Ratnasamy P (1990) Appl Catal 58:L1
4. Reddy JS, Kumar R (1991) J Catal 130:440
5. Notari B (1996) Adv Catal 41:253
6. Gallot JE, Kaliaguine S (1998) Can J Chem Eng 76:833
7. Kresge CT, Leonowicz ME, Roth WJ, Vartuli JC, Beck JS (1992) Nature 359:710
8. Huo QS, Margolese DI, Ciesla U, Demuth DG, Feng PY, Gier TE, Sieger P, Firouzi A, Chmelka BF, Schuth F, Stucky GD (1994) Chem Mater 6:1176
9. Wan Y, Shi YF, Zhao D (2007) Chem Commun 897
10. Wan Y, Zhao D (2007) Chem Rev 107:2821
11. Soler-Illia GJAA, Sanchez C, Lebeau B, Patarin J (2002) Chem Rev 102:4093
12. Zhao D, Feng J, Huo Q, Melosh N, Fredrickson GH, Chmelka BF, Stucky GD (1998) Science 279:548
13. Zhao D, Huo Q, Feng J, Chmelka BF, Stucky GD (1998) J Am Chem Soc 120:6024
14. Khodakov AY, Zholobenko VL, Bechara R, Durant D (2005) Micropor Mesopor Mater 79:29
15. Linssen T, Cassiers K, Cool P, Vansant EF (2003) Adv Colloid Interface Sci 103:121
16. On DT, Desplantier-Giscard D, Danumah C, Kaliaguine S (2003) Appl Catal A 253:543
17. Taguchi A, Schüth F (2005) Micropor Mesopor Mater 77:1
18. Corma A (1997) Chem Rev 97:2373
19. Moller K, Bein T (1998) Chem Mater 10:2950
20. Arends IWCE, Sheldon RA (2001) Appl Catal A 212:175
21. Fryxell GE (2006) Inorg Chem Commun 9:1141
22. Oye G, Glomm WR, Vralstad T, Volden S, Magnusson H, Stocker M, Sjoblom J (2003) Adv Colloid Interface Sci 123:17
23. Ungureanu A, On DT, Dimitriu E, Kaliaguine S (2003) Appl Catal A 254:203
24. Dubé D, Royer S, On DT, Béland F, Kaliaguine S (2005) Micropor Mesopor Mater 79:137
25. Wu P, Iwamoto MJ (1998) Chem Soc Faraday Trans 94:2871
26. Chiker F, Nogier JP, Launay F, Bonardet JL (2003) Appl Catal A 243:309
27. Widenmeyer M, Grasser S, Köhler K, Anwander R (2001) Micropor Mesopor Mater 44–45:327
28. Kim MJ, Chang SH, Choi JS, Ahn WS (2004) React Kinet Catal Lett 82:27
29. Luan Z, Maes EM, van der Heide PAW, Zhao D, Czernuszewicz RS, Kevan L (1999) Chem Mater 11:3680
30. Brutchey RL, Mork BV, Sirbuly DJ, Yang P, Tilley TD (2005) J Mol Catal A 238:1
31. Ferreira P, Gonçalves IS, Kühn FE, Pillinger M, Rocha J, Santos AM, Thursfield A (2000) Eur J Inorg Chem 551
32. Pérez Y, Pérez Quintanilla D, Fajardo M, Sierra I, del Hierro I (2007) J Mol Catal A 271:227
33. Oldroyd RD, Thomas JM, Maschmeyer T, MacFaul PA, Snelgrove DW, Ingold KU, Wayner DDM (1996) Angew Chem Int Ed 35:2787
34. Blasco T, Corma A, Navarro MT, Pérez Pariente J (1995) J Catal 156:65
35. Koyano KA, Tatsumi T (1997) Micropor Mater 10:259
36. Maschmeyer T, Rey F, Sankar G, Thomas JM (1995) Nature 387:159
37. Koyano KA, Tatsumi T (1996) Chem Commun 145
38. Corma A, Kan Q, Rey F (1998) Chem Commun 579
39. Morey M, Davidson A, Stucky G (1996) Micropor Mater 6:99
40. Morey MS, O'Brien S, Schwarz S, Stucky GD (2000) Chem Mater 12:898
41. Zhang W, Fröba M, Wang J, Tanev PT, Wong J, Pinnavaia TJ (1996) J Am Chem Soc 118:9164
42. Tuel A (1999) Micropor Mesopor Mater 27:151
43. Bagshaw SA, Prouzet E, Pinnavaia TJ (1995) Science 269:1242
44. Bagshaw SA, Di Renzo F, Fajula F (1996) Chem Commun 2209
45. Bagshaw SA, Kemmitt T, Milestone NB (1998) Micropor Mesopor Mater 22:419
46. Ji D, Ren T, Yan L, Suo J (2003) Mater Lett 57:4474
47. Ji D, Zhao R, Lv G, Qian G, Yan L, Suo J (2005) Appl Catal A 281:39
48. Vinu A, Srinivasu P, Sawant DP, Alam S, Mori T, Ariga K, Balasubramanian VV, Anand C (2008) Micropor Mesopor Mater 110:422
49. Zhang WH, Lu J, Han B, Li M, Xiu J, Ying P, Li C (2002) Chem Mater 14:3413
50. Newalkar BL, Olanrewaju J, Komarneni S (2001) Chem Mater 13:552
51. Wu S, Han Y, Zou YC, Song JW, Zhao L, Di Y, Liu SZ, Xiao FS (2004) Chem Mater 16:486
52. Berube F, Kleitz F, Kaliaguine S (2008) J Phys Chem C 112:14403
53. Vinu A, Srinivasu P, Miyahara M, Ariga K (2006) J Phys Chem B 110:801
54. Chen Y, Huang Y, Xiu J, Han X, Bao X (2004) Appl Catal A 273:185
55. Trukhan NN, Romannikov VN, Shmakov AN, Vanina MP, Paukshtis EA, Bukhtiyarov VI, Kriventsov VV, Danilov IY, Kholdeeva OA (2003) Micropor Mesopor Mater 59:73
56. Ravikovitch PI, Neimark AV (2001) J Phys Chem B 105:6817
57. Hua Z, Bu W, Lian Y, Chen H, Li L, Zhang L, Li C, Shi J (2005) J Mater Chem 15:661

58. Galarneau A, Cambon H, Di Renzo F, Fajula F (2001) Langmuir 17:8328
59. Ryoo R, Ko CH, Kruk M, Antochshuk V, Jaroniec M (2000) J Phys Chem B 104:11465
60. Hoang VT, Huang Q, Eic M, Do TO, Kaliaguine S (2005) Langmuir 21:2051
61. Gobin OC, Wan Y, Zhao D, Kleitz F, Kaliaguine S (2007) J Phys Chem C 111:3053
62. Geobaldo CF, Bordiga S, Zecchina A, Giamello E, Leofanti G, Petrini G (1992) Catal Lett 16:109
63. On DT, Le Noc L, Bonneviot L (1996) Chem Commun 299
64. On DT, Kapoor MP, Kaliaguine S (1996) Chem Commun 1161
65. Tozzola G, Mantegazza MA, Ranghino G, Petrini G, Bordiga S, Ricchiardi G, Lamberti C, Zulian R, Zecchina A (1998) J Catal 179:64
66. Deo G, Turek AM, Wachs IE, Huybrechts DRC, Jacobs PA (1993) Zeolites 13:365
67. Stakheev AY, Shpiro ES, Apijok J (1993) J Phys Chem 97:5663
68. Kaliaguine S (1996) Stud Surf Sci Catal 102:191
69. Notari B (1988) Stud Surf Sci Catal 37:413
70. Klein S, Thorimbert S, Maier WF (1996) J Catal 163:476